

Experimental study of $\psi(2S)$ decays to $K^+K^-\pi^+\pi^-\pi^0$ final states

M. Ablikim¹, J. Z. Bai¹, Y. Ban¹², J. G. Bian¹, X. Cai¹, H. F. Chen¹⁷, H. S. Chen¹,
H. X. Chen¹, J. C. Chen¹, Jin Chen¹, Y. B. Chen¹, S. P. Chi², Y. P. Chu¹,
X. Z. Cui¹, Y. S. Dai¹⁹, L. Y. Diao⁹, Z. Y. Deng¹, Q. F. Dong¹⁵, S. X. Du¹,
J. Fang¹, S. S. Fang², C. D. Fu¹, C. S. Gao¹, Y. N. Gao¹⁵, S. D. Gu¹, Y. T. Gu⁴,
Y. N. Guo¹, Y. Q. Guo¹, Z. J. Guo¹⁶, F. A. Harris¹⁶, K. L. He¹, M. He¹³,
Y. K. Heng¹, H. M. Hu¹, T. Hu¹, G. S. Huang^{1a}, X. T. Huang¹³, X. B. Ji¹,
X. S. Jiang¹, X. Y. Jiang⁵, J. B. Jiao¹³, D. P. Jin¹, S. Jin¹, Yi Jin⁸, Y. F. Lai¹,
G. Li², H. B. Li¹, H. H. Li¹, J. Li¹, R. Y. Li¹, S. M. Li¹, W. D. Li¹, W. G. Li¹,
X. L. Li¹, X. N. Li¹, X. Q. Li¹¹, Y. L. Li⁴, Y. F. Liang¹⁴, H. B. Liao¹, B. J. Liu¹,
C. X. Liu¹, F. Liu⁶, Fang Liu¹, H. H. Liu¹, H. M. Liu¹, J. Liu¹², J. B. Liu¹,
J. P. Liu¹⁸, Q. Liu¹, R. G. Liu¹, Z. A. Liu¹, Y. C. Lou⁵, F. Lu¹, G. R. Lu⁵,
J. G. Lu¹, C. L. Luo¹⁰, F. C. Ma⁹, H. L. Ma¹, L. L. Ma¹, Q. M. Ma¹, X. B. Ma⁵,
Z. P. Mao¹, X. H. Mo¹, J. Nie¹, S. L. Olsen¹⁶, H. P. Peng^{17b}, R. G. Ping¹,
N. D. Qi¹, H. Qin¹, J. F. Qiu¹, Z. Y. Ren¹, G. Rong¹, L. Y. Shan¹, L. Shang¹,
C. P. Shen¹, D. L. Shen¹, X. Y. Shen¹, H. Y. Sheng¹, H. S. Sun¹, J. F. Sun¹,
S. S. Sun¹, Y. Z. Sun¹, Z. J. Sun¹, Z. Q. Tan⁴, X. Tang¹, G. L. Tong¹,
G. S. Varner¹⁶, D. Y. Wang¹, L. Wang¹, L. L. Wang¹, L. S. Wang¹, M. Wang¹,
P. Wang¹, P. L. Wang¹, W. F. Wang^{1c}, Y. F. Wang¹, Z. Wang¹, Z. Y. Wang¹,
Zhe Wang¹, Zheng Wang², C. L. Wei¹, D. H. Wei¹, N. Wu¹, X. M. Xia¹,
X. X. Xie¹, G. F. Xu¹, X. P. Xu⁶, Y. Xu¹¹, M. L. Yan¹⁷, H. X. Yang¹, Y. X. Yang³,
M. H. Ye², Y. X. Ye¹⁷, Z. Y. Yi¹, G. W. Yu¹, C. Z. Yuan¹, J. M. Yuan¹, Y. Yuan¹,
S. L. Zang¹, Y. Zeng⁷, Yu Zeng¹, B. X. Zhang¹, B. Y. Zhang¹, C. C. Zhang¹,
D. H. Zhang¹, H. Q. Zhang¹, H. Y. Zhang¹, J. W. Zhang¹, J. Y. Zhang¹,
S. H. Zhang¹, X. M. Zhang¹, X. Y. Zhang¹³, Yiyun Zhang¹⁴, Z. P. Zhang¹⁷,
D. X. Zhao¹, J. W. Zhao¹, M. G. Zhao¹, P. P. Zhao¹, W. R. Zhao¹, Z. G. Zhao^{1d},
H. Q. Zheng¹², J. P. Zheng¹, Z. P. Zheng¹, L. Zhou¹, N. F. Zhou^{1d}, K. J. Zhu¹,
Q. M. Zhu¹, Y. C. Zhu¹, Y. S. Zhu¹, Yingchun Zhu^{1b}, Z. A. Zhu¹, B. A. Zhuang¹,
X. A. Zhuang¹, B. S. Zou¹

(BES Collaboration)

- ¹ *Institute of High Energy Physics, Beijing 100049, People's Republic of China*
- ² *China Center for Advanced Science and Technology(CCAST), Beijing 100080, People's Republic of China*
- ³ *Guangxi Normal University, Guilin 541004, People's Republic of China*
- ⁴ *Guangxi University, Nanning 530004, People's Republic of China*
- ⁵ *Henan Normal University, Xinxiang 453002, People's Republic of China*
- ⁶ *Huazhong Normal University, Wuhan 430079, People's Republic of China*
- ⁷ *Hunan University, Changsha 410082, People's Republic of China*
- ⁸ *Jinan University, Jinan 250022, People's Republic of China*
- ⁹ *Liaoning University, Shenyang 110036, People's Republic of China*
- ¹⁰ *Nanjing Normal University, Nanjing 210097, People's Republic of China*
- ¹¹ *Nankai University, Tianjin 300071, People's Republic of China*
- ¹² *Peking University, Beijing 100871, People's Republic of China*
- ¹³ *Shandong University, Jinan 250100, People's Republic of China*
- ¹⁴ *Sichuan University, Chengdu 610064, People's Republic of China*
- ¹⁵ *Tsinghua University, Beijing 100084, People's Republic of China*
- ¹⁶ *University of Hawaii, Honolulu, HI 96822, USA*
- ¹⁷ *University of Science and Technology of China, Hefei 230026, People's Republic of China*
- ¹⁸ *Wuhan University, Wuhan 430072, People's Republic of China*
- ¹⁹ *Zhejiang University, Hangzhou 310028, People's Republic of China*
- ^a *Current address: Purdue University, West Lafayette, IN 47907, USA*
- ^b *Current address: DESY, D-22607, Hamburg, Germany*
- ^c *Current address: Laboratoire de l'Accélérateur Linéaire, Orsay, F-91898, France*
- ^d *Current address: University of Michigan, Ann Arbor, MI 48109, USA*

$K^+K^-\pi^+\pi^-\pi^0$ final states are studied using a sample of 14×10^6 $\psi(2S)$ decays collected with the Beijing Spectrometer (BESII) at the Beijing Electron-Positron Collider. The branching fractions of $\psi(2S)$ decays to $K^+K^-\pi^+\pi^-\pi^0$, ωK^+K^- , $\omega f_0(1710)$, $K^*(892)^0 K^-\pi^+\pi^0 + c.c.$, $K^*(892)^+ K^-\pi^+\pi^- + c.c.$, $K^*(892)^+ K^-\rho^0 +$

$c.c.$ and $K^*(892)^0 K^- \rho^+ + c.c.$ are determined. The first two agree with previous measurements, and the last five are first measurements.

PACS numbers: 13.25.Gv, 14.40.Cs, 13.40.Hq

I. INTRODUCTION

From perturbative QCD (pQCD), it is expected that both J/ψ and $\psi(2S)$ decaying into light hadrons are dominated by the annihilation of $c\bar{c}$ into three gluons, with widths proportional to the square of the wave function at the origin $|\Psi(0)|^2$ [1]. This yields the pQCD “12%” rule:

$$Q_h = \frac{B_{\psi(2S) \rightarrow h}}{B_{J/\psi \rightarrow h}} \approx \frac{B_{\psi(2S) \rightarrow e^+e^-}}{B_{J/\psi \rightarrow e^+e^-}} \approx 12\%.$$

The violation of the above rule was first observed in the $\rho\pi$ and $K^{*+}K^- + c.c.$ decay modes by Mark-II [2]. Following the scenario proposed in Ref. [3], that the small $\psi(2S) \rightarrow \rho\pi$ branching fraction is due to the cancelation of the S- and D-wave matrix elements in $\psi(2S)$ decays, it was suggested that all $\psi(2S)$ decay channels should be affected by the same S- and D-wave mixing scheme, and thus all ratios of branching fractions of $\psi(2S)$ and J/ψ decays into the same final state could have values different from 12%, expected between pure 1S and 2S states [4]. The mixing scenario also predicts $\psi(3770)$ decay branching fractions since the $\psi(3770)$ is a mixture of S- and D-wave charmonia, as well. Many channels of J/ψ , $\psi(2S)$ decays, and $\psi(3770)$ decays should be measured to test this scenario.

In this paper, we report measurements of $K^+K^-\pi^+\pi^-\pi^0$ final states, as well as some intermediate states that decay to the same final states. The data samples used for this analysis consist of $14.0 \times 10^6(1 \pm 4\%)$ $\psi(2S)$ events taken at $\sqrt{s} = 3.686$ GeV [5] and $6.42(1 \pm 4\%) \text{pb}^{-1}$ of continuum data at $\sqrt{s} = 3.65$ GeV [6].

II. BESII DETECTOR

BESII is a large solid-angle magnetic spectrometer which is described in detail in Ref. [7]. The momentum of charged particles is determined by a 40-layer cylindrical main drift chamber (MDC) which has a momentum resolution of $\sigma_p/p=1.78\%\sqrt{1+p^2}$ (p in GeV/c). Particle identification (PID) is accomplished using specific ionization (dE/dx) measurements in the drift chamber and time-of-flight (TOF) information in a barrel-like array of 48 scintillation counters. The dE/dx resolution is $\sigma_{dE/dx} \simeq 8.0\%$; the TOF resolution for Bhabha events is $\sigma_{TOF} = 180$ ps. Radially outside of the time-of-flight counters is a 12-radiation-length barrel shower counter (BSC) comprised of gas tubes interleaved with lead sheets. The BSC measures the energy and direction of photons with resolutions of $\sigma_E/E \simeq 21\%/\sqrt{E}$ (E in GeV), $\sigma_\phi = 7.9$ mrad, and $\sigma_z = 2.3$ cm. The iron flux return of the magnet is instrumented with three double layers of proportional counters that are used to identify muons.

A GEANT3 based Monte Carlo (MC) simulation package [8], which simulates the detector response, including interactions of secondary particles in the detector material, is used to determine detection efficiencies and mass resolutions, as well as to optimize selection criteria and estimate backgrounds. Reasonable agreement between data and MC simulation is observed in various channels tested, including $e^+e^- \rightarrow (\gamma)e^+e^-$, $e^+e^- \rightarrow (\gamma)\mu^+\mu^-$, $J/\psi \rightarrow p\bar{p}$, $J/\psi \rightarrow \rho\pi$, and $\psi(2S) \rightarrow \pi^+\pi^-J/\psi$, $J/\psi \rightarrow l^+l^-$.

III. EVENT SELECTION

The $K^+K^-\pi^+\pi^-\pi^0$ final states are reconstructed with four charged tracks and two photons.

A. Photon and charged particle identification

A neutral cluster is considered to be a good photon candidate if the following requirements are satisfied: it is located within the BSC fiducial region, the energy

deposited in the BSC is greater than 50 MeV, the first hit appears in the first six-radiation lengths, the angle between the cluster development direction in the BSC and the photon emission direction is less than 37° , and the angle between the cluster and the nearest charged particle is greater than 15° .

Each charged track is required to be well fit by a three dimensional helix, to originate from the interaction region, $V_{xy} = \sqrt{V_x^2 + V_y^2} < 2.0$ cm and $|V_z| < 20$ cm, and to have a polar angle $|\cos\theta| < 0.8$. Here V_x , V_y , and V_z are the x , y , z coordinates of the point of closest approach of the track to the beam axis. The TOF and dE/dx measurements for each charged track are used to calculate $\chi_{PID}^2(i)$ values and the corresponding confidence levels $Prob_{PID}(i)$ for the hypotheses that a track is a pion, kaon, or proton, where i ($i = \pi/K/p$) is the particle type.

B. Selection criteria

For the final states of interest, the candidate events are required to satisfy the following selection criteria:

1. The number of charged tracks in the MDC equals four with net charge zero.
2. The number of good photon candidates equals two or three.
3. For each charged track, the particle identification confidence level for a candidate particle assignment is required to be greater than 1%.
4. The angle between two photons satisfies $\theta_{\gamma\gamma} > 6^\circ$ to remove the background from split-off fake photons.
5. To reduce contamination from $\psi(2S) \rightarrow \eta J/\psi$ with $\eta \rightarrow \pi^+\pi^-\pi^0$ and $J/\psi \rightarrow \mu^+\mu^-$, $N_+^{hit} + N_-^{hit} < 4$ is used, where N_+^{hit} is the number of muon identification layers with matched hits for the higher momentum positive charged track and ranges from 0 to 3, indicating not a muon (0) or a weakly (1), moderately (2), or strongly (3) identified muon [9], and N_-^{hit} is the corresponding number for the higher momentum negative charged track.

6. To reject background from $\psi(2S) \rightarrow \pi^+\pi^-J/\psi$, $|M_{recoil}^{\pi^+\pi^-} - 3.097| > 0.05$ GeV/ c^2 is used, where $M_{recoil}^{\pi^+\pi^-}$ is the mass recoiling against the $\pi^+\pi^-$ pair.

To improve track momentum resolution and reduce background, four constraint kinematic fits imposing energy and momentum conservation are performed. We loop over all combinations of charged tracks and good photons and select the one with the minimum χ_{com}^2 for the assignment $\psi(2S) \rightarrow \gamma\gamma\pi^+\pi^-K^+K^-$, where the combined χ^2 , χ_{com}^2 , is defined as the sum of the χ^2 values of the kinematic fit, χ_{kine}^2 , and those from each of the four particle identification assignments: $\chi_{com}^2 = \sum_i \chi_{PID}^2(i) + \chi_{kine}^2$. We require $\chi_{com}^2(\gamma\gamma\pi^+\pi^-K^+K^-) < \chi_{com}^2(\gamma\gamma\pi^+\pi^-\pi^+\pi^-)$, $\chi_{com}^2(\gamma\gamma\pi^+\pi^-K^+K^-) < \chi_{com}^2(\gamma\gamma K^+K^-K^+K^-)$, and the confidence level of the kinematic fit to be greater than 1%.

After applying the above selection criteria, there is still background remaining from $\psi(2S) \rightarrow K_S K^\pm \pi^\mp \pi^0$, $K_S \rightarrow \pi^+\pi^-$. This is removed by requiring $m_{\pi^+\pi^-} > 0.51$ GeV/ c^2 or $m_{\pi^+\pi^-} < 0.45$ GeV/ c^2 , $m_{K^+\pi^-} > 0.51$ GeV/ c^2 or $m_{K^+\pi^-} < 0.47$ GeV/ c^2 , and $m_{K^-\pi^+} > 0.51$ GeV/ c^2 or $m_{K^-\pi^+} < 0.47$ GeV/ c^2 , where in calculating $m_{K\pi}$, the π mass is used for the K^\pm track.

IV. DATA ANALYSIS

The $\gamma\gamma$ invariant mass distribution for events that survive the selection criteria is shown in Fig. 1(a), where a clear π^0 signal can be seen. By fitting this distribution with a π^0 signal shape, obtained from MC simulation, and a 3rd order background polynomial, 698 ± 41 events are obtained in the $\sqrt{s} = 3.686$ GeV data sample. From exclusive Monte Carlo simulation, we determine that the main background channels are from $\psi(2S) \rightarrow \pi^0\pi^0J/\psi$, $J/\psi \rightarrow K^+K^-\pi^+\pi^-$, $\psi(2S) \rightarrow \gamma\chi_{cJ}$, $\chi_{cJ} \rightarrow K^+K^-\pi^+\pi^-$, and $\psi(2S) \rightarrow \gamma\chi_{cJ}$, $\chi_{cJ} \rightarrow K^+K^-\pi^+\pi^-\pi^0$. However, the $\gamma\gamma$ invariant mass distributions from all these background channels do not have a peak at $m_{\gamma\gamma} = m_{\pi^0}$, and, therefore, they will not contribute to the number of fitted events. Applying the same selection criteria to the $\sqrt{s} = 3.65$ GeV data, we obtain the $\gamma\gamma$ invariant mass distribution shown in Fig. 1(b). Fitting Fig. 1(b) in a similar way as Fig. 1(a) yields 35 ± 7 events. The efficiencies are $(3.68 \pm 0.05)\%$ for $\psi(2S) \rightarrow K^+K^-\pi^+\pi^-\pi^0$

and $(2.59 \pm 0.05)\%$ for continuum $e^+e^- \rightarrow K^+K^-\pi^+\pi^-\pi^0$, where the difference is due to the initial state radiation for continuum data. Here in calculating efficiencies, we have considered the contributions from important intermediate states (shown later in the paper) in $\psi(2S) \rightarrow K^+K^-\pi^+\pi^-\pi^0$.

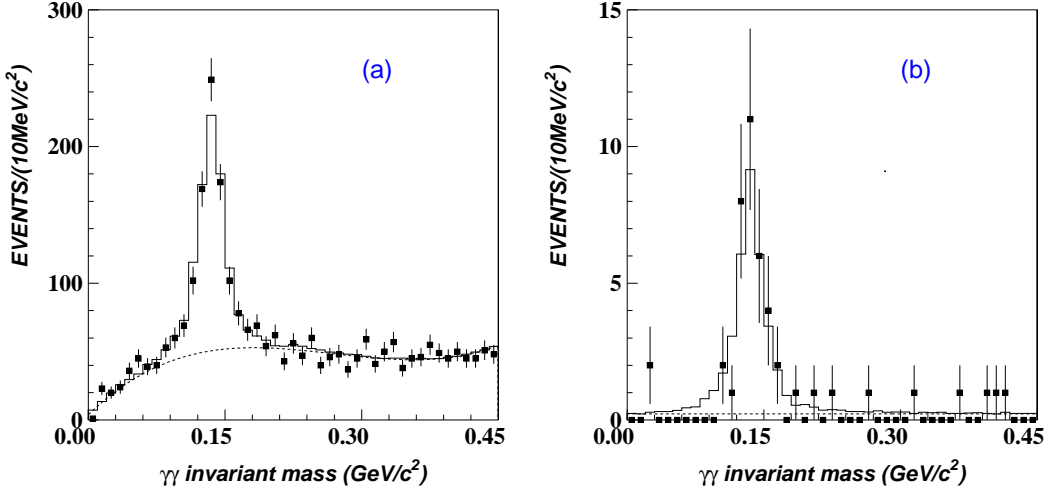


FIG. 1: The $\gamma\gamma$ invariant mass distributions of (a) selected $\psi(2S) \rightarrow K^+K^-\pi^+\pi^-\gamma\gamma$ candidate events and (b) selected $e^+e^- \rightarrow K^+K^-\pi^+\pi^-\gamma\gamma$ candidate events at $\sqrt{s} = 3.65$ GeV. The squares with error bars are data, the histograms are the fit, and the dashed curves are background shapes from the fit.

In the following analysis, we study the $\pi^+\pi^-\pi^0$, K^+K^- , $K^+\pi^- + c.c.$, $K^+\pi^0 + c.c.$ and $\pi^+\pi^-$ invariant mass spectra to look for possible intermediate resonance states. Fig. 2(a) shows the $\pi^+\pi^-\pi^0$ invariant mass distribution for $K^+K^-\pi^+\pi^-\gamma\gamma$ events after requiring $|m_{\gamma\gamma} - 0.135| < 0.03$ GeV/ c^2 (to increase the efficiency, the requirements on $m_{\pi^+\pi^-}$ and $m_{K\pi}$ used for the K_S veto are removed); a clear ω signal is observed. A fit with an ω signal shape obtained from MC simulation and a polynomial background gives 78 ± 11 signal events with a statistical significance of 8.0σ . The detection efficiency for this decay mode is $(2.66 \pm 0.04)\%$, where we have considered the contributions from important intermediate states. Fig. 2(b) shows the $\pi^+\pi^-\pi^0$ invariant mass distribution for $\sqrt{s} = 3.65$ GeV data, where we obtain $0_{-0}^{+1.3}$ ωK^+K^- events at the 68.3% confidence level with a similar fit to the $\pi^+\pi^-\pi^0$ invariant mass spectrum.

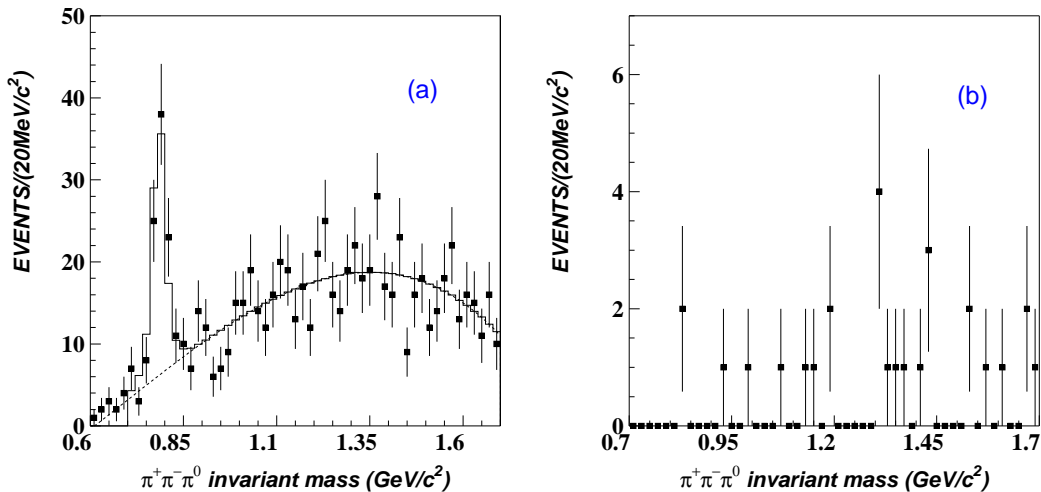


FIG. 2: The $\pi^+\pi^-\pi^0$ invariant mass distributions of (a) selected $\psi(2S) \rightarrow K^+K^-\pi^+\pi^-\pi^0$ candidate events and (b) selected $e^+e^- \rightarrow K^+K^-\pi^+\pi^-\pi^0$ candidate events at $\sqrt{s} = 3.65$ GeV. The squares with error bars are data, the histograms are the fit, and the dashed curves are background shapes from the fit.

The Dalitz plot of events satisfying $|m_{\pi^+\pi^-\pi^0} - m_\omega| < 0.04$ GeV/ c^2 is shown in Fig. 3(a). There are vertical and horizontal directions bands corresponding to $K_1(1270)^\pm \rightarrow \omega K^\pm$, and a diagonal band corresponding to a K^+K^- resonance. After requiring $m_{\omega K} > 1.5$ GeV/ c^2 to remove the $K_1(1270)^\pm$, the K^+K^- invariant mass distribution is shown in Fig. 3(b). There is a cluster of events near 1.7 GeV/ c^2 , and there is no similar structure in ω sideband events ($0.06 < m_{\pi^+\pi^-\pi^0} - m_\omega < 0.1$ GeV/ c^2 or $-0.1 < m_{\pi^+\pi^-\pi^0} - m_\omega < -0.06$ GeV/ c^2), as shown in the hatched histogram. Assuming the peak is $f_0(1710)$, a fit with the mass fixed at 1.714 GeV/ c^2 and width fixed at 140 MeV/ c^2 [10] gives 18.9 ± 6.2 events. The statistical significance for $\psi(2S) \rightarrow \omega f_0(1710)$ is 3.7σ , and the detection efficiency for this decay mode is $(2.62 \pm 0.06)\%$. No signal for $e^+e^- \rightarrow \omega f_0(1710)$ is observed at $\sqrt{s} = 3.65$ GeV.

After requiring $|m_{\pi^+\pi^-\pi^0} - 0.783| > 0.04$ GeV/ c^2 to remove $\psi(2S) \rightarrow \omega K^+K^-$ events, the $K^\pm\pi^\mp$ mass distributions of $K^+K^-\pi^+\pi^-\pi^0$ candidates are shown in Fig. 4 for (a) $\sqrt{s} = 3.686$ GeV data and (b) $\sqrt{s} = 3.65$ GeV data. By fitting the $K\pi$ invariant mass spectrum with the Monte Carlo determined shape for signal, the $K\pi$ mass distribution of π^0 sideband events ($0.18 < m_{\gamma\gamma} < 0.21$ GeV/ c^2 or $0.06 < m_{\gamma\gamma} <$

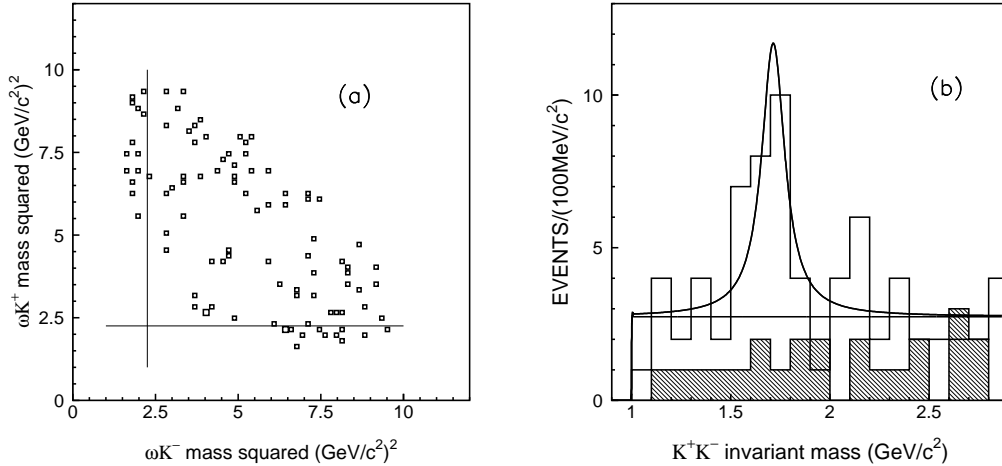


FIG. 3: (a) The Dalitz plot of selected $\psi(2S) \rightarrow \omega K^+ K^-$ candidates, and (b) the $K^+ K^-$ invariant mass distribution for candidate $\psi(2S) \rightarrow \omega K^+ K^-$ events after the $K_1(1270)$ veto ($m_{\omega K} > 1.5 \text{ GeV}/c^2$). The hatched histogram is from ω sidebands, and the curves in (b) show the fit described in the text.

0.09 GeV/c^2) to describe the peaking background (mainly $\gamma K^*(892)^0 K^- \pi^+ + c.c.$), and a Legendre polynomial for other backgrounds, as shown in Fig. 4(a), 281 ± 30 events at $\sqrt{s} = 3.686 \text{ GeV}$ for $K^*(892)^0 K^- \pi^+ \pi^0 + c.c.$ are obtained. For the continuum data, the peaking background is negligible, and the fit is performed with a signal shape and a Legendre background polynomial and yields 15 ± 5 events, as shown in Fig. 4(b). Similarly, the $K^\pm \pi^0$ mass distributions are shown in Fig. 5, and 150 ± 26 events at $\sqrt{s} = 3.686 \text{ GeV}$ and 6 ± 5 events at $\sqrt{s} = 3.65 \text{ GeV}$ are obtained for $K^*(892)^+ K^- \pi^+ \pi^- + c.c.$, as shown in Figs. 5(a) and (b). After subtracting the continuum contributions, we obtain 238 ± 34 events for $\psi(2S) \rightarrow K^*(892)^0 K^- \pi^+ \pi^0 + c.c.$ with a detection efficiency of $(3.00 \pm 0.06)\%$ and 133 ± 30 events for $\psi(2S) \rightarrow K^*(892)^+ K^- \pi^+ \pi^- + c.c.$ with a detection efficiency of $(3.02 \pm 0.06)\%$.

The $\pi^+ \pi^-$ invariant mass distributions after requiring $|m_{K^\pm \pi^0} - 0.896| < 0.06 \text{ GeV}/c^2$ are shown in Fig. 6. The spectra are fitted with Monte Carlo determined ρ shapes and Legendre background polynomials, as shown in Figs. 6(a) and (b), and the fit yields 92 ± 19 events at $\sqrt{s} = 3.686 \text{ GeV}$ and 5 ± 4 events at $\sqrt{s} = 3.65 \text{ GeV}$ for $K^*(892)^+ K^- \rho^0 + c.c.$. Similarly the $\pi^\pm \pi^0$ invariant mass distributions are shown

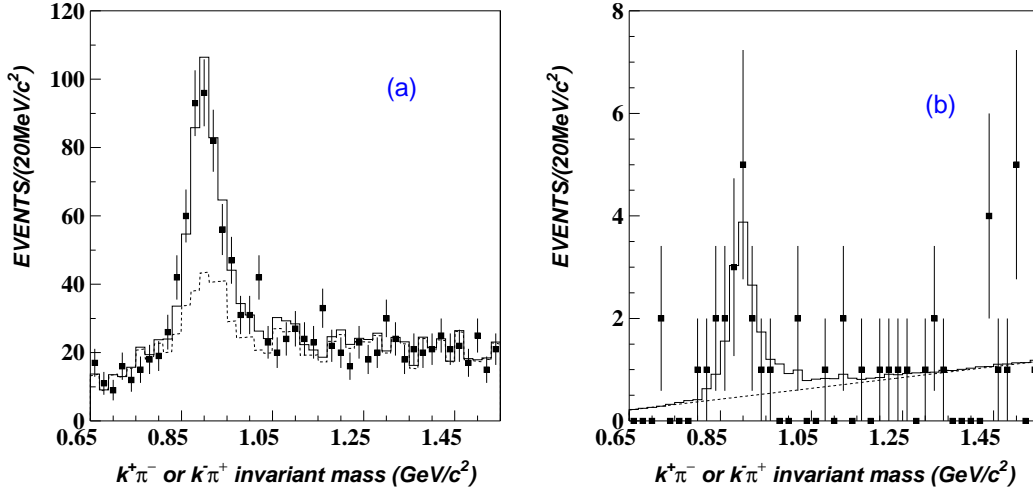


FIG. 4: $K^\pm\pi^\mp$ invariant mass distributions for $K^+K^-\pi^+\pi^-\pi^0$ candidate events from (a) $\sqrt{s} = 3.686$ GeV data and (b) $\sqrt{s} = 3.65$ GeV data. The squares with error bars are data, the histograms are the fit, and the dashed lines are the sum of the $K\pi$ mass distribution from π^0 sideband events and a Legendre polynomial.

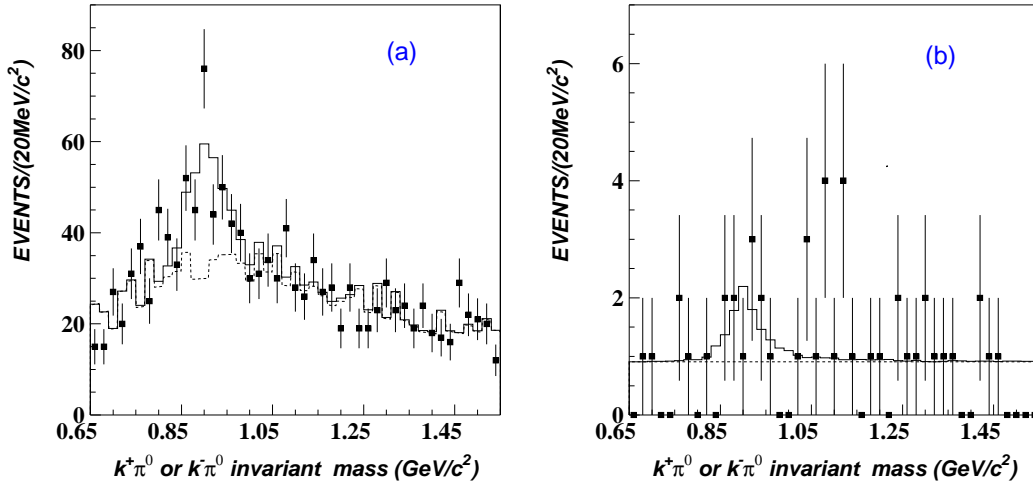


FIG. 5: $K^\pm\pi^0$ invariant mass distributions for $K^+K^-\pi^+\pi^-\pi^0$ candidate events from (a) $\sqrt{s} = 3.686$ GeV data and (b) $\sqrt{s} = 3.65$ GeV data. The squares with error bars are data, the histograms are the fit, and the dashed lines are the sum of the $K\pi$ mass distribution from π^0 sideband events and a Legendre polynomial.

in Fig. 7 for the $\sqrt{s} = 3.686$ GeV and $\sqrt{s} = 3.65$ GeV data samples. The fits, shown in Figs. 7(a) and (b), yield 142 ± 23 events at $\sqrt{s} = 3.686$ GeV and 6 ± 4 events at $\sqrt{s} = 3.65$ GeV for $K^*(892)^0 K^- \rho^+ + c.c.$. After subtracting the continuum contributions, we obtain 78 ± 23 $\psi(2S) \rightarrow K^*(892)^+ K^- \rho^0 + c.c.$ events with a detection efficiency of $(2.32 \pm 0.05)\%$ and 125 ± 26 $\psi(2S) \rightarrow K^*(892)^0 K^- \rho^+ + c.c.$ events with a detection efficiency of $(2.24 \pm 0.05)\%$.

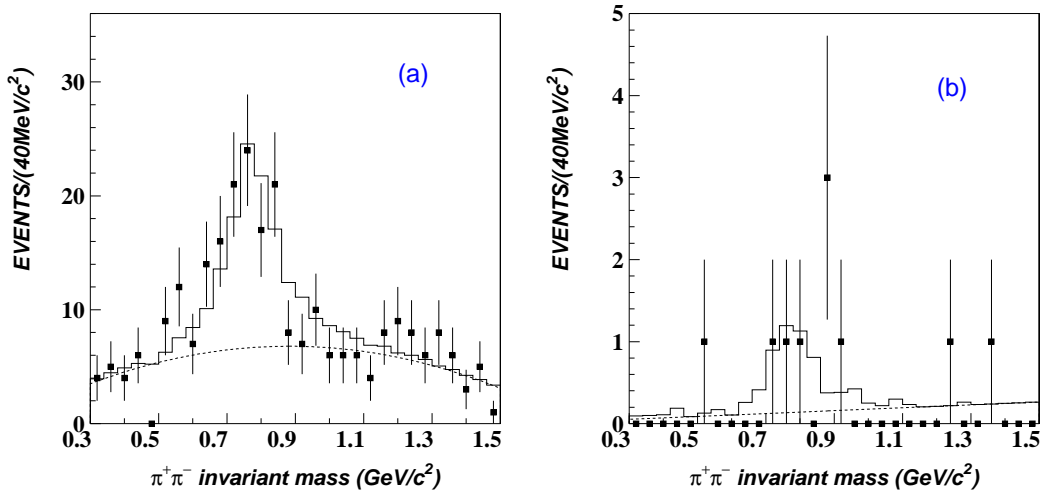


FIG. 6: $\pi^+\pi^-$ invariant mass distributions from (a) $\sqrt{s} = 3.686$ GeV data and (b) $\sqrt{s} = 3.65$ GeV data for $K^*(892)^+ K^- \pi^+\pi^- + c.c.$ candidate events. The squares with error bars are data, the histograms are the fit, and the dashed curves are background shapes from the fit.

After requiring $|m_{K\pi} - 0.896| < 0.06$ GeV/ c^2 and $|m_{\pi\pi} - m_\rho| < 0.15$ GeV/ c^2 , the Dalitz plots of $\psi(2S) \rightarrow K^*(892)^+ K^- \rho^0 + c.c.$ and $\psi(2S) \rightarrow K^*(892)^0 K^- \rho^+ + c.c.$ candidates are shown in Figs. 8(a) and (b), where no further clear structures are observed.

V. SYSTEMATIC ERRORS

Systematic errors on the branching fractions mainly originate from the MC statistics, the track error matrix, the kinematic fit, particle identification, the photon efficiency, the uncertainty of the branching fractions of the intermediate states (from

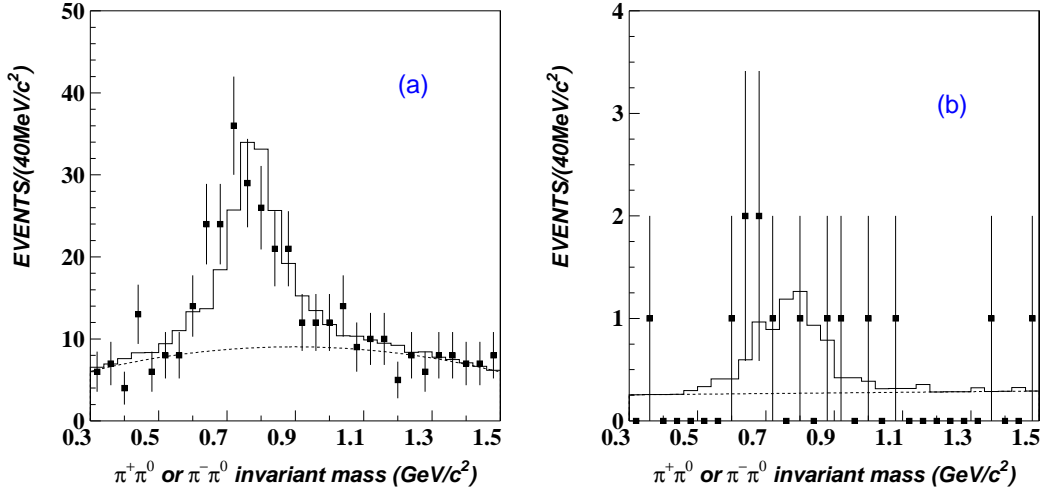


FIG. 7: $\pi^\pm\pi^0$ invariant mass distributions from (a) $\sqrt{s} = 3.686$ GeV data and (b) $\sqrt{s} = 3.65$ GeV data for $K^*(892)^0 K^- \pi^+ \pi^0 + c.c.$ candidate events. The squares with error bars are data, the histograms are the fit, and the dashed curves are background shapes from the fit.

PDG) [10], the $K^*(892)$ simulation, the fitting, and the total number of $\psi(2S)$ events.

1. The MDC tracking efficiency was measured using clean channels like $J/\psi \rightarrow \Lambda\bar{\Lambda}$ and $\psi(2S) \rightarrow \pi^+\pi^- J/\psi$, $J/\psi \rightarrow \mu^+\mu^-$. It is found that the MC simulation agrees with data within (1–2)% for each charged track. Therefore, 8% is taken as the systematic error for events with four charged tracks.
2. The photon detection efficiency was studied using different methods with $J/\psi \rightarrow \pi^+\pi^-\pi^0$ events [8], and the difference between data and MC simulation is about 2% for each photon. The systematic error due to the differences between data and Monte Carlo simulation of fake photons and the reconstruction of the π^0 is less than 2.5% [11]. We take 5% as the systematic error for channels with two photons.
3. The systematic error associated with the kinematic fit is caused by differences between the momenta and error matrices from track fitting of the charged tracks and the energies and the directions of the neutral tracks for data and

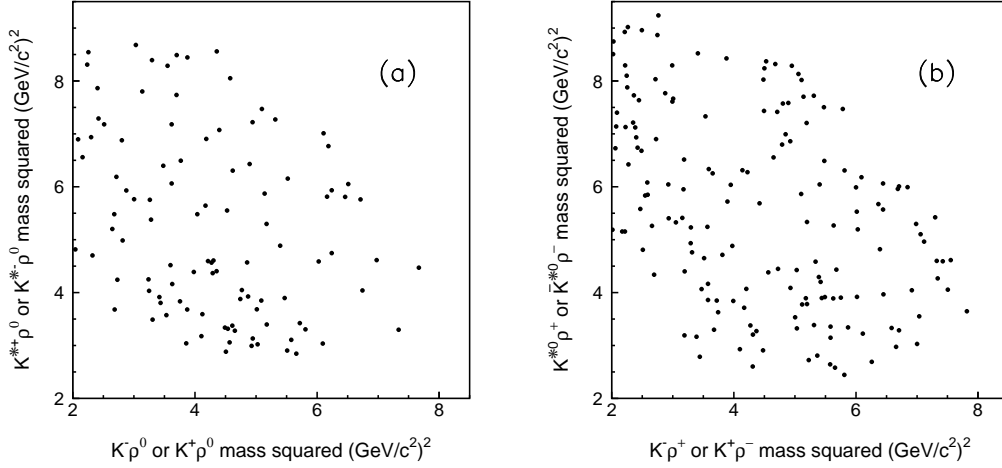


FIG. 8: Dalitz plots of (a) $\psi(2S) \rightarrow K^*(892)^+K^-\rho^0 + c.c.$ and (b) $\psi(2S) \rightarrow K^*(892)^0K^-\rho^+ + c.c.$

Monte Carlo data. For the channels analyzed, $Prob(\chi^2, 4) > 0.01$ is required, and we take 4% as the systematic error from the kinematic fit [12]. Fig. 9 shows the comparison of the χ^2 distributions for data and MC sample, where we require $|m_{\gamma\gamma} - 0.135| < 0.03$ GeV/ c^2 and subtract π^0 sideband background. MC simulation agrees with data within large statistical uncertainty of the data sample.

4. The background uncertainties in the $K^+K^-\pi^+\pi^-\pi^0$, ωK^+K^- , $\omega f_0(1710)$, $K^*(892)^0K^-\pi^+\pi^0 + c.c.$, $K^*(892)^+K^-\pi^+\pi^- + c.c.$, $K^*(892)^+K^-\rho^0 + c.c.$, and $K^*(892)^0K^-\rho^+ + c.c.$ channels are estimated to be about 1.5%, 1.6%, 1.6%, 7.1%, 9.5%, 11.4%, and 11.3%, respectively, by changing the order of the polynomial and the fitting range used. Varying the mass and width of the $f_0(1710)$ [13] in the fit yields a change in the number of $\omega f_0(1710)$ events by 8.6%. Together with the background uncertainty, we take 8.8% as the systematic error for $\psi(2S) \rightarrow \omega f_0(1710)$ due to fitting.
5. Pure π and K samples were selected, and the particle identification efficiency was measured as a function of the track momentum. On the average, a 1.3% efficiency difference per π track and a 1.0% difference per K track are

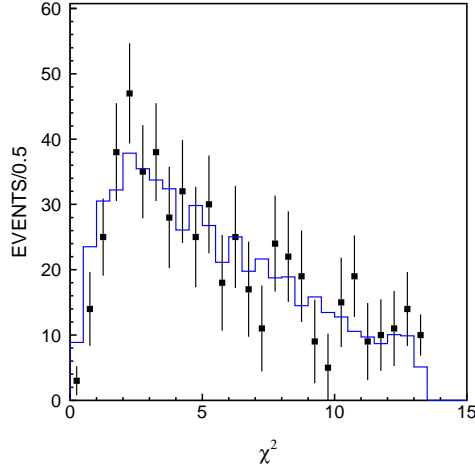


FIG. 9: The χ^2 distribution from the kinematic fit. The squares with error bars are data, and the histogram is MC simulated $\psi(2S) \rightarrow K^+K^-\pi^+\pi^-\pi^0$.

observed between data and MC simulation. The total systematic error for $K^+K^-\pi^+\pi^-\pi^0$ is taken as 4.6%.

6. The $K^*(892)$ is simulated with a P-wave relativistic Breit-Wigner function, with the width $\Gamma = \Gamma_0 \frac{m_0}{m} \frac{1+r^2 p_0^2}{1+r^2 p^2} \left[\frac{p}{p_0} \right]^3$, where r is the interaction radius and the value $(3.4 \pm 0.6 \pm 0.3) (\text{GeV}/c)^{-1}$ measured by a $K^-\pi^+$ scattering experiment [14] is used as an estimation of the interaction radius. Varying the value of r by 1σ , the detection efficiencies for $\psi(2S)$ decaying to $K^*(892)^0 K^-\pi^+\pi^0 + c.c.$, $K^*(892)^+ K^-\pi^+\pi^- + c.c.$, $K^*(892)^+ K^-\rho^0 + c.c.$, and $K^*(892)^0 K^-\rho^+ + c.c.$ changed by 3.0% for the first two modes and 7.0% for the last two modes, which are taken as systematic errors for the uncertainty of the r value.
7. For the $K^*(892)^0 K^-\pi^+\pi^0 + c.c.$ decay mode, there are backgrounds that also peak in the signal region of the $K\pi$ mass plot. The largest is from $\gamma K^*(892)^0 K^-\pi^+ + c.c.$ events combined with fake photons. We use π^0 sideband events to estimate these background contributions. In the analysis, the π^0 sideband range is from 3 to 5 σ , where σ is 15 MeV/ c^2 . If the π^0 sideband range is chosen between 5 and 7 σ , the difference with the standard sideband is 8.0%. If the π^0 sideband range is from 2 to 3 σ , the difference is 13.7%. So

we take 13.7% as the systematic error due to the π^0 sideband definition in the fitting. Using a similar procedure for $K^*(892)^+K^-\pi^+\pi^- + c.c.$ decay, 8.1% is determined as the systematic error.

8. In calculating the Born order cross section for $e^+e^- \rightarrow K^+K^-\pi^+\pi^-\pi^0$, the error for the integrated luminosity is 4%. The other systematic errors are similar to those for $\psi(2S) \rightarrow K^+K^-\pi^+\pi^-\pi^0$. The total systematic error for $\sigma(e^+e^- \rightarrow K^+K^-\pi^+\pi^-\pi^0)$ is 12.1%.

Table I lists all the systematic errors from different sources, the total systematic errors for $\psi(2S) \rightarrow K^+K^-\pi^+\pi^-\pi^0$, $\psi(2S) \rightarrow \omega K^+K^-$, $\psi(2S) \rightarrow \omega f_0(1710)$, $\psi(2S) \rightarrow K^{*0}K^-\pi^+\pi^0 + c.c.$, $\psi(2S) \rightarrow K^{*+}K^-\pi^+\pi^- + c.c.$, $\psi(2S) \rightarrow K^{*+}K^-\rho^0 + c.c.$ and $\psi(2S) \rightarrow K^{*0}K^-\rho^+ + c.c.$ are 12.1%, 12.2%, 15.1%, 19.9%, 17.7%, 18.1% and 18.1% respectively.

TABLE I: Summary of systematic errors (%). Errors common to all modes are only listed once.

Source	$K^+K^-\pi^+\pi^-\pi^0$	ωK^+K^-	$\omega f_0(1710)$	$K^{*0}K^-\pi^+\pi^0$	$K^{*+}K^-\pi^+\pi^-$	$K^{*+}K^-\rho^0$	$K^{*0}K^-\rho^+$
				<i>c.c.</i>	<i>c.c.</i>	<i>c.c.</i>	<i>c.c.</i>
MC statistics	1.4	1.5	2.3	2.0	1.8	2.2	2.3
Tracking efficiency				8.0			
Kinematic fit				4.0			
PID efficiency				4.6			
Photon ID and π^0 reconstruction				5.0			
Fitting	1.5	1.6	8.8	7.1	9.5	11.4	11.3
Branching fractions	...	0.8	0.8
r uncertainty	3.0	3.0	7.0	7.0
π^0 sideband	13.7	8.1
$N_{\psi(2S)}$				4.0			
Sum	12.1	12.2	15.1	19.9	17.7	18.1	18.1

VI. RESULTS AND DISCUSSION

To obtain the branching fraction of $\psi(2S) \rightarrow X$, we must subtract the contribution from the continuum process. This is estimated using continuum data at

$\sqrt{s} = 3.65$ GeV, normalized by f :

$$f = \frac{\mathcal{L}_{3.686} \times \sigma_{3.686}^{cont}}{\mathcal{L}_{3.650} \times \sigma_{3.650}^{cont}},$$

where $\mathcal{L}_{\sqrt{s}}$ is the integrated luminosity at \sqrt{s} , and $\sigma_{\sqrt{s}}^{cont}$ is the Born order cross section of the continuum process at \sqrt{s} , which is s dependent and can be expressed in terms of a form factor $\mathcal{F}(s)$:

$$\sigma_{\sqrt{s}}^{cont} = \frac{4\pi\alpha^2}{3s} \times |\mathcal{F}(s)|^2, \quad (1)$$

where α is the QED fine structure constant. Assuming $|\mathcal{F}(s)| \propto 1/s$, we get $f = 2.89$. The branching fraction of $\psi(2S) \rightarrow X$ can be calculated from

$$\mathcal{B}[\psi(2S) \rightarrow X] = \frac{N_{3.686}^{obs} - N_{3.650}^{obs} \times f}{\varepsilon_{\psi(2S)} \times N_{\psi(2S)}^{tot} \times B(X \rightarrow Y)},$$

where X is the intermediate state and Y is the final state.

Using the numbers obtained above and listed in Table II, we get

$$B(\psi(2S) \rightarrow K^+K^-\pi^+\pi^-\pi^0) = (1.17 \pm 0.10 \pm 0.15) \times 10^{-3},$$

$$B(\psi(2S) \rightarrow \omega K^+K^-) = (2.38 \pm 0.37 \pm 0.29) \times 10^{-4},$$

$$B(\psi(2S) \rightarrow \omega f_0(1710), f_0(1710) \rightarrow K^+K^-) = (5.9 \pm 2.0 \pm 0.9) \times 10^{-5},$$

$$B(\psi(2S) \rightarrow K^*(892)^0 K^-\pi^+\pi^0 + c.c.) = (8.6 \pm 1.3 \pm 1.8) \times 10^{-4},$$

$$B(\psi(2S) \rightarrow K^*(892)^+ K^-\pi^+\pi^- + c.c.) = (9.6 \pm 2.2 \pm 1.7) \times 10^{-4},$$

$$B(\psi(2S) \rightarrow K^*(892)^+ K^-\rho^0 + c.c.) = (7.3 \pm 2.2 \pm 1.4) \times 10^{-4},$$

$$B(\psi(2S) \rightarrow K^*(892)^0 K^-\rho^+ + c.c.) = (6.1 \pm 1.3 \pm 1.2) \times 10^{-4},$$

where the first errors are statistical and the second are systematic. The measured $\psi(2S) \rightarrow K^+K^-\pi^+\pi^-\pi^0$ branching fraction agrees well with the value of $(1.27 \pm 0.05 \pm 0.10) \times 10^{-3}$ obtained by CLEO [15], and the $\psi(2S) \rightarrow \omega K^+K^-$ branching fraction agrees with BES1 [16] and CLEO results within 1.5σ . The other five modes are first observations.

The Born order cross section for $e^+e^- \rightarrow K^+K^-\pi^+\pi^-\pi^0$ at $\sqrt{s} = 3.65$ GeV is

$$\sigma_{e^+e^- \rightarrow K^+K^-\pi^+\pi^-\pi^0}^B = \frac{N^{obs}}{\mathcal{L}\epsilon(1+\delta)} = (171 \pm 35 \pm 21) \text{ pb},$$

TABLE II: Numbers used in the branching fraction calculations. The number of events due to $\psi(2S)$ decay, $N_{\psi(2S)}^{obs}$, is computed according to $N_{3.686}^{obs} - f \times N_{3.65}^{obs}$.

Quantity	$K^+K^-\pi^+\pi^-\pi^0$	ωK^+K^-	$\omega f_0(1710)$	$K^{*0}K^-\pi^+\pi^0$	$K^{*+}K^-\pi^+\pi^-$	$K^{*+}K^-\rho^0$	$K^{*0}K^-\rho^+$
				+c.c.	+c.c.	+c.c.	+c.c.
$N_{3.65}^{obs}$	35 ± 7	$0_{-0}^{+1.3}$	–	15 ± 5	6 ± 5	5 ± 4	6 ± 4
$N_{3.686}^{obs}$	698 ± 41	78 ± 11	18.9 ± 6.2	281 ± 30	150 ± 26	92 ± 19	142 ± 23
$N_{\psi(2S)}^{obs}$	597 ± 46	78_{-11}^{+12}	18.9 ± 6.2	238 ± 34	133 ± 30	78 ± 23	125 ± 26
$\epsilon(\%)$	3.68 ± 0.05	2.66 ± 0.04	2.62 ± 0.06	3.00 ± 0.06	3.02 ± 0.06	2.32 ± 0.05	2.24 ± 0.05
$N_{\psi(2S)}(10^6)$	$14(1 \pm 4\%)$						

where ϵ is the detection efficiency obtained from the MC simulation, \mathcal{L} is the integrated luminosity and $1 + \delta$ is the radiative correction factor which is 1.23 [17].

To test the 12% rule, we also list in Table III the ratio Q_h of the $\psi(2S)$ and J/ψ branching fractions for the three channels $\psi(2S) \rightarrow K^+K^-\pi^+\pi^-\pi^0$, $\psi(2S) \rightarrow \omega K^+K^-$, and $\psi(2S) \rightarrow \omega f_0(1710)$, $f_0(1710) \rightarrow K^+K^-$. $B(J/\psi \rightarrow K^+K^-\pi^+\pi^-\pi^0)$ is taken from the PDG [10], while the values on $B(J/\psi \rightarrow \omega K^+K^-)$ and $B(J/\psi \rightarrow \omega f_0(1710))$ come from Ref. [13], a recent measurement using a partial wave analysis and the BESII J/ψ sample. All three modes obey the 12% rule within 1σ . The four modes with K^* we observed in $\psi(2S)$ decays are not measured in J/ψ decays, so Q_h values can not be computed.

TABLE III: Branching fractions for $\psi(2S)$ and J/ψ hadronic decays and Q_h values. The errors are the quadratic sum of the statistical and systematic errors.

Channel	$B_{\psi(2S) \rightarrow h}(10^{-4})$	$B_{J/\psi \rightarrow h}(10^{-4})$	$Q_h(\%)$
$K^+K^-\pi^+\pi^-\pi^0$	11.7 ± 1.8	120 ± 28 [10]	9.8 ± 2.8
ωK^+K^-	2.38 ± 0.47	16.8 ± 2.1 [13]	14.2 ± 3.4
$\omega f_0(1710) \rightarrow \omega K^+K^-$	0.59 ± 0.22	6.6 ± 1.3 [13]	8.9 ± 3.8

VII. ACKNOWLEDGMENT

The BES collaboration thanks the staff of BEPC for their hard efforts. This work is supported in part by the National Natural Science Foundation of China under contracts Nos. 10491300, 10225524, 10225525, 10425523, the Chinese Academy of Sciences under contract No. KJ 95T-03, the 100 Talents Program of CAS under Contract Nos. U-11, U-24, U-25, and the Knowledge Innovation Project of CAS under Contract Nos. U-602, U-34 (IHEP), the National Natural Science Foundation of China under Contract No. 10225522 (Tsinghua University), and the Department of Energy under Contract No. DE-FG02-04ER41291 (U Hawaii).

-
- [1] T. Appelquist and H. D. Politzer, Phys. Rev. Lett. **34**, 43 (1975); A. De Rújula and S. L. Glashow, Phys. Rev. Lett. **34**, 46 (1975).
 - [2] Mark-II Collab., M. E. B. Franklin *et al.*, Phys. Rev. Lett. **51**, 963 (1983).
 - [3] J. L. Rosner, Phys. Rev. D **64**, 094002 (2001).
 - [4] P. Wang, C. Z. Yuan and X. H. Mo, Phys. Rev. D **70**, 114014 (2004).
 - [5] X. H. Mo *et al.*, High Energy Phys. Nucl. Phys. **28**, 455 (2004), hep-ex/0407055.
 - [6] S. P. Chi, X. H. Mo and Y. S. Zhu, High Energy Phys. Nucl. Phys. **28**, 1135 (2004).
 - [7] BES Collab., J. Z. Bai *et al.*, Nucl. Instrum. Methods A **458**, 627 (2001).
 - [8] BES Collab., M. Ablikim *et al.*, Nucl. Instrum. Methods A **552**, 344 (2005).
 - [9] BES Collab., J. Z. Bai *et al.*, High Energy Phys. Nucl. Phys. **20**, 97 (1996).
 - [10] S. Eidelman *et al.* (Particle Data Group), Phys. Lett. B **592**, 1 (2004).
 - [11] BES Collab., M. Ablikim *et al.*, Phys. Rev. D **71**, 072006 (2005).
 - [12] BES Collab., J. Z. Bai *et al.*, Phys. Rev. D **69**, 072001 (2004).
 - [13] BES Collab., J. Z. Bai *et al.*, Phys. Lett. B **603**, 138 (2004). The branching fraction of $B(J/\psi \rightarrow \omega K^+ K^-)$ is calculated using the numbers in this paper, the total error for $\psi(2S) \rightarrow \omega f_0(1710)$ is 19.7% and the $f_0(1710)$ intensity is $(38 \pm 6)\%$ of the data, where the error is almost entirely systematic. So we estimated the systematic error for $J/\psi \rightarrow \omega K^+ K^-$ is 11.8%.
 - [14] D. Aston *et al.*, Nucl. Phys. B **296**, 493 (1988).

- [15] CLEO Collab., R. A. Briere *et al.*, Phys. Rev. Lett. **95**, 062001 (2005).
- [16] BES Collab., J. Z. Bai *et al.*, Phys. Rev. D **67**, 052002 (2003).
- [17] G. Bonneau and F. Martin, Nucl. Phys. B **27**, 381 (1971).